

Search for the radiative leptonic decay $D^+ \rightarrow \gamma e^+ \nu_e$

M. Ablikim,¹ M. N. Achasov,^{9,8} S. Ahmed,¹⁴ X. C. Ai,¹ O. Albayrak,⁵ M. Albrecht,⁴ D. J. Ambrose,⁴⁵ A. Amoroso,^{50a,50c}
 F. F. An,¹ Q. An,^{47,38} J. Z. Bai,¹ O. Bakina,²³ R. Baldini Ferroli,^{20a} Y. Ban,³¹ D. W. Bennett,¹⁹ J. V. Bennett,⁵ N. Berger,²²
 M. Bertani,^{20a} D. Bettoni,^{21a} J. M. Bian,⁴⁴ F. Bianchi,^{50a,50c} E. Boger,^{23,†} I. Boyko,²³ R. A. Briere,⁵ H. Cai,⁵² X. Cai,^{1,38}
 O. Cakir,^{41a} A. Calcaterra,^{20a} G. F. Cao,^{1,42} S. A. Cetin,^{41b} J. Chai,^{50c} J. F. Chang,^{1,38} G. Chelkov,^{23,†,‡} G. Chen,¹
 H. S. Chen,^{1,42} J. C. Chen,¹ M. L. Chen,^{1,38} S. Chen,⁴² S. J. Chen,²⁹ X. Chen,^{1,38} X. R. Chen,²⁶ Y. B. Chen,^{1,38} X. K. Chu,³¹
 G. Cibinetto,^{21a} H. L. Dai,^{1,38} J. P. Dai,^{34,††} A. Dbeyssi,¹⁴ D. Dedovich,²³ Z. Y. Deng,¹ A. Denig,²² I. Denysenko,²³
 M. Destefanis,^{50a,50c} F. De Mori,^{50a,50c} Y. Ding,²⁷ C. Dong,³⁰ J. Dong,^{1,38} L. Y. Dong,^{1,42} M. Y. Dong,^{1,38,42} Z. L. Dou,²⁹
 S. X. Du,⁵⁴ P. F. Duan,¹ J. Z. Fan,⁴⁰ J. Fang,^{1,38} S. S. Fang,^{1,42} X. Fang,^{47,38} Y. Fang,¹ R. Farinelli,^{21a,21b} L. Fava,^{50b,50c}
 S. Fegan,²² F. Feldbauer,²² G. Felici,^{20a} C. Q. Feng,^{47,38} E. Fioravanti,^{21a} M. Fritsch,^{22,14} C. D. Fu,¹ Q. Gao,¹ X. L. Gao,^{47,38}
 Y. Gao,⁴⁰ Z. Gao,^{47,38} I. Garzia,^{21a} K. Goetzen,¹⁰ L. Gong,³⁰ W. X. Gong,^{1,38} W. Gradl,²² M. Greco,^{50a,50c} M. H. Gu,^{1,38}
 Y. T. Gu,¹² Y. H. Guan,¹ A. Q. Guo,¹ L. B. Guo,²⁸ R. P. Guo,¹ Y. Guo,¹ Y. P. Guo,²² Z. Haddadi,²⁵ A. Hafner,²² S. Han,⁵²
 X. Q. Hao,¹⁵ F. A. Harris,⁴³ K. L. He,^{1,42} F. H. Heinsius,⁴ T. Held,⁴ Y. K. Heng,^{1,38,42} T. Holtmann,⁴ Z. L. Hou,¹ C. Hu,²⁸
 H. M. Hu,^{1,42} T. Hu,^{1,38,42} Y. Hu,¹ G. S. Huang,^{47,38} J. S. Huang,¹⁵ X. T. Huang,³³ X. Z. Huang,²⁹ Z. L. Huang,²⁷
 T. Hussain,⁴⁹ W. Ikegami Andersson,⁵¹ Q. Ji,¹ Q. P. Ji,¹⁵ X. B. Ji,^{1,42} X. L. Ji,^{1,38} L. W. Jiang,⁵² X. S. Jiang,^{1,38,42}
 X. Y. Jiang,³⁰ J. B. Jiao,³³ Z. Jiao,¹⁷ D. P. Jin,^{1,38,42} S. Jin,^{1,42} T. Johansson,⁵¹ A. Julin,⁴⁴ N. Kalantar-Nayestanaki,²⁵
 X. L. Kang,¹ X. S. Kang,³⁰ M. Kavatsyuk,²⁵ B. C. Ke,⁵ P. Kiese,²² R. Kliemt,¹⁰ B. Kloss,²² O. B. Kolcu,^{41b,¶} B. Kopf,⁴
 M. Kornicer,⁴³ A. Kupsc,⁵¹ W. Kühn,²⁴ J. S. Lange,²⁴ M. Lara,¹⁹ P. Larin,¹⁴ H. Leithoff,²² C. Leng,^{50c} C. Li,⁵¹ Cheng Li,^{47,38}
 D. M. Li,⁵⁴ F. Li,^{1,38} F. Y. Li,³¹ G. Li,¹ H. B. Li,^{1,42} H. J. Li,¹ J. C. Li,¹ Jin Li,³² K. Li,¹³ K. Li,³³ Lei Li,³ P. L. Li,^{47,38}
 P. R. Li,^{42,7} Q. Y. Li,³³ T. Li,³³ W. D. Li,^{1,42} W. G. Li,¹ X. L. Li,³³ X. N. Li,^{1,38} X. Q. Li,³⁰ Y. B. Li,² Z. B. Li,³⁹ H. Liang,^{47,38}
 Y. F. Liang,³⁶ Y. T. Liang,²⁴ G. R. Liao,¹¹ D. X. Lin,¹⁴ B. Liu,^{34,††} B. J. Liu,¹ C. X. Liu,¹ D. Liu,^{47,38} F. H. Liu,³⁵ Fang Liu,¹
 Feng Liu,⁶ H. B. Liu,¹² H. H. Liu,¹⁶ H. H. Liu,¹ H. M. Liu,^{1,42} J. Liu,¹ J. B. Liu,^{47,38} J. P. Liu,⁵² J. Y. Liu,¹ K. Liu,⁴⁰
 K. Y. Liu,²⁷ L. D. Liu,³¹ P. L. Liu,^{1,38} Q. Liu,⁴² S. B. Liu,^{47,38} X. Liu,²⁶ Y. B. Liu,³⁰ Y. Y. Liu,³⁰ Z. A. Liu,^{1,38,42} Zhiqing Liu,²²
 H. Loehner,²⁵ Y. F. Long,³¹ X. C. Lou,^{1,38,42} H. J. Lu,¹⁷ J. G. Lu,^{1,38} Y. Lu,¹ Y. P. Lu,^{1,38} C. L. Luo,²⁸ M. X. Luo,⁵³ T. Luo,⁴³
 X. L. Luo,^{1,38} X. R. Lyu,⁴² F. C. Ma,²⁷ H. L. Ma,¹ L. L. Ma,³³ M. M. Ma,¹ Q. M. Ma,¹ T. Ma,¹ X. N. Ma,³⁰ X. Y. Ma,^{1,38}
 Y. M. Ma,³³ F. E. Maas,¹⁴ M. Maggiora,^{50a,50c} Q. A. Malik,⁴⁹ Y. J. Mao,³¹ Z. P. Mao,¹ S. Marcello,^{50a,50c}
 J. G. Messchendorp,²⁵ G. Mezzadri,^{21b} J. Min,^{1,38} T. J. Min,¹ R. E. Mitchell,¹⁹ X. H. Mo,^{1,38,42} Y. J. Mo,⁶
 C. Morales Morales,¹⁴ G. Morello,^{20a} N. Yu. Muchnoi,^{9,8} H. Muramatsu,⁴⁴ P. Musiol,⁴ Y. Nefedov,²³ F. Nerling,¹⁰
 I. B. Nikolaev,^{9,8} Z. Ning,^{1,38} S. Nisar,⁸ S. L. Niu,^{1,38} X. Y. Niu,¹ S. L. Olsen,³² Q. Ouyang,^{1,38,42} S. Pacetti,^{20b} Y. Pan,^{47,38}
 M. Papenbrock,⁵¹ P. Patteri,^{20a} M. Pelizaeus,⁴ H. P. Peng,^{47,38} K. Peters,^{10,**} J. Pettersson,⁵¹ J. L. Ping,²⁸ R. G. Ping,^{1,42}
 R. Poling,⁴⁴ V. Prasad,¹ H. R. Qi,² M. Qi,²⁹ S. Qian,^{1,38} C. F. Qiao,⁴² L. Q. Qin,³³ N. Qin,⁵² X. S. Qin,¹ Z. H. Qin,^{1,38}
 J. F. Qiu,¹ K. H. Rashid,^{49,‡‡} C. F. Redmer,²² M. Ripka,²² G. Rong,^{1,42} Ch. Rosner,¹⁴ X. D. Ruan,¹² A. Sarantsev,^{23,||}
 M. Savrié,^{21b} C. Schnier,⁴ K. Schoenning,⁵¹ W. Shan,³¹ M. Shao,^{47,38} C. P. Shen,² P. X. Shen,³⁰ X. Y. Shen,^{1,42} H. Y. Sheng,¹
 W. M. Song,¹ X. Y. Song,¹ S. Sosio,^{50a,50c} S. Spataro,^{50a,50c} G. X. Sun,¹ J. F. Sun,¹⁵ S. S. Sun,^{1,42} X. H. Sun,¹ Y. J. Sun,^{47,38}
 Y. Z. Sun,¹ Z. J. Sun,^{1,38} Z. T. Sun,¹⁹ C. J. Tang,³⁶ X. Tang,¹ I. Tapan,^{41c} E. H. Thorndike,⁴⁵ M. Tiemens,²⁵ I. Uman,^{41d}
 G. S. Varner,⁴³ B. Wang,³⁰ B. L. Wang,⁴² D. Wang,³¹ D. Y. Wang,³¹ K. Wang,^{1,38} L. L. Wang,¹ L. S. Wang,¹ M. Wang,³³
 P. Wang,¹ P. L. Wang,¹ W. Wang,^{1,38} W. P. Wang,^{47,38} X. F. Wang,⁴⁰ Y. Wang,³⁷ Y. D. Wang,¹⁴ Y. F. Wang,^{1,38,42}
 Y. Q. Wang,²² Z. Wang,^{1,38} Z. G. Wang,^{1,38} Z. H. Wang,^{47,38} Z. Y. Wang,¹ Z. Y. Wang,¹ T. Weber,²² D. H. Wei,¹¹
 P. Weidenkaff,²² S. P. Wen,¹ U. Wiedner,⁴ M. Wolke,⁵¹ L. H. Wu,¹ L. J. Wu,¹ Z. Wu,^{1,38} L. Xia,^{47,38} L. G. Xia,⁴⁰ Y. Xia,¹⁸
 D. Xiao,¹ H. Xiao,⁴⁸ Z. J. Xiao,²⁸ Y. G. Xie,^{1,38} Y. H. Xie,⁶ Q. L. Xiu,^{1,38} G. F. Xu,¹ J. J. Xu,¹ L. Xu,¹ Q. J. Xu,¹³ Q. N. Xu,⁴²
 X. P. Xu,³⁷ L. Yan,^{50a,50c} W. B. Yan,^{47,38} W. C. Yan,^{47,38} Y. H. Yan,¹⁸ H. J. Yang,^{34,††} H. X. Yang,¹ L. Yang,⁵² Y. X. Yang,¹¹
 M. Ye,^{1,38} M. H. Ye,⁷ J. H. Yin,¹ Z. Y. You,³⁹ B. X. Yu,^{1,38,42} C. X. Yu,³⁰ J. S. Yu,²⁶ C. Z. Yuan,^{1,42} Y. Yuan,¹ A. Yuncu,^{41b,*}
 A. A. Zafar,⁴⁹ Y. Zeng,¹⁸ Z. Zeng,^{47,38} B. X. Zhang,¹ B. Y. Zhang,^{1,38} C. C. Zhang,¹ D. H. Zhang,¹ H. H. Zhang,³⁹
 H. Y. Zhang,^{1,38} J. Zhang,¹ J. J. Zhang,¹ J. L. Zhang,¹ J. Q. Zhang,¹ J. W. Zhang,^{1,38,42} J. Y. Zhang,¹ J. Z. Zhang,^{1,42}
 K. Zhang,¹ L. Zhang,¹ S. Q. Zhang,³⁰ X. Y. Zhang,³³ Y. Zhang,¹ Y. Zhang,¹ Y. H. Zhang,^{1,38} Y. N. Zhang,⁴² Y. T. Zhang,^{47,38}
 Yu Zhang,⁴² Z. H. Zhang,⁶ Z. P. Zhang,⁴⁷ Z. Y. Zhang,⁵² G. Zhao,¹ J. W. Zhao,^{1,38} J. Y. Zhao,¹ J. Z. Zhao,^{1,38} Lei Zhao,^{47,38}
 Ling Zhao,¹ M. G. Zhao,³⁰ Q. Zhao,¹ Q. W. Zhao,¹ S. J. Zhao,⁵⁴ T. C. Zhao,¹ Y. B. Zhao,^{1,38} Z. G. Zhao,^{47,38}
 A. Zhemchugov,^{23,†} B. Zheng,^{48,14} J. P. Zheng,^{1,38} W. J. Zheng,³³ Y. H. Zheng,⁴² B. Zhong,²⁸ L. Zhou,^{1,38} X. Zhou,⁵²
 X. K. Zhou,^{47,38} X. R. Zhou,^{47,38} X. Y. Zhou,¹ K. Zhu,¹ K. J. Zhu,^{1,38,42} S. Zhu,¹ S. H. Zhu,⁴⁶ X. L. Zhu,⁴⁰ Y. C. Zhu,^{47,38}
 Y. S. Zhu,^{1,42} Z. A. Zhu,^{1,42} J. Zhuang,^{1,38} L. Zotti,^{50a,50c} B. S. Zou,¹ and J. H. Zou¹

(BESIII Collaboration)

¹Institute of High Energy Physics, Beijing 100049, People's Republic of China²Beihang University, Beijing 100191, People's Republic of China

- ³Beijing Institute of Petrochemical Technology, Beijing 102617, People's Republic of China
⁴Bochum Ruhr-University, D-44780 Bochum, Germany
⁵Carnegie Mellon University, Pittsburgh, Pennsylvania 15213, USA
⁶Central China Normal University, Wuhan 430079, People's Republic of China
⁷China Center of Advanced Science and Technology, Beijing 100190, People's Republic of China
⁸COMSATS Institute of Information Technology,
Lahore, Defence Road, Off Raiwind Road, 54000 Lahore, Pakistan
⁹G. I. Budker Institute of Nuclear Physics SB RAS (BINP), Novosibirsk 630090, Russia
¹⁰GSI Helmholtzcentre for Heavy Ion Research GmbH, D-64291 Darmstadt, Germany
¹¹Guangxi Normal University, Guilin 541004, People's Republic of China
¹²Guangxi University, Nanning 530004, People's Republic of China
¹³Hangzhou Normal University, Hangzhou 310036, People's Republic of China
¹⁴Helmholtz Institute Mainz, Johann-Joachim-Becher-Weg 45, D-55099 Mainz, Germany
¹⁵Henan Normal University, Xinxiang 453007, People's Republic of China
¹⁶Henan University of Science and Technology, Luoyang 471003, People's Republic of China
¹⁷Huangshan College, Huangshan 245000, People's Republic of China
¹⁸Human University, Changsha 410082, People's Republic of China
¹⁹Indiana University, Bloomington, Indiana 47405, USA
^{20a}INFN Laboratori Nazionali di Frascati, I-00044, Frascati, Italy
^{20b}INFN and University of Perugia, I-06100, Perugia, Italy
^{21a}INFN Sezione di Ferrara, I-44122, Ferrara, Italy
^{21b}University of Ferrara, I-44122, Ferrara, Italy
²²Johannes Gutenberg University of Mainz, Johann-Joachim-Becher-Weg 45, D-55099 Mainz, Germany
²³Joint Institute for Nuclear Research, 141980 Dubna, Moscow region, Russia
²⁴Justus-Liebig-Universitaet Giessen,
II. Physikalisches Institut, Heinrich-Buff-Ring 16, D-35392 Giessen, Germany
²⁵KVI-CART, University of Groningen, NL-9747 AA Groningen, Netherlands
²⁶Lanzhou University, Lanzhou 730000, People's Republic of China
²⁷Liaoning University, Shenyang 110036, People's Republic of China
²⁸Nanjing Normal University, Nanjing 210023, People's Republic of China
²⁹Nanjing University, Nanjing 210093, People's Republic of China
³⁰Nankai University, Tianjin 300071, People's Republic of China
³¹Peking University, Beijing 100871, People's Republic of China
³²Seoul National University, Seoul 151-747, Korea
³³Shandong University, Jinan 250100, People's Republic of China
³⁴Shanghai Jiao Tong University, Shanghai 200240, People's Republic of China
³⁵Shanxi University, Taiyuan 030006, People's Republic of China
³⁶Sichuan University, Chengdu 610064, People's Republic of China
³⁷Soochow University, Suzhou 215006, People's Republic of China
³⁸State Key Laboratory of Particle Detection and Electronics,
Beijing 100049, Hefei 230026, People's Republic of China
³⁹Sun Yat-Sen University, Guangzhou 510275, People's Republic of China
⁴⁰Tsinghua University, Beijing 100084, People's Republic of China
^{41a}Ankara University, 06100 Tandogan, Ankara, Turkey
^{41b}Istanbul Bilgi University, 34060 Eyup, Istanbul, Turkey
^{41c}Uludag University, 16059 Bursa, Turkey
^{41d}Near East University, Nicosia, North Cyprus, Mersin 10, Turkey
⁴²University of Chinese Academy of Sciences, Beijing 100049, People's Republic of China
⁴³University of Hawaii, Honolulu, Hawaii 96822, USA
⁴⁴University of Minnesota, Minneapolis, Minnesota 55455, USA
⁴⁵University of Rochester, Rochester, New York 14627, USA
⁴⁶University of Science and Technology Liaoning, Anshan 114051, People's Republic of China
⁴⁷University of Science and Technology of China, Hefei 230026, People's Republic of China
⁴⁸University of South China, Hengyang 421001, People's Republic of China
⁴⁹University of the Punjab, Lahore-54590, Pakistan
^{50a}University of Turin, I-10125, Turin, Italy
^{50b}University of Eastern Piedmont, I-15121, Alessandria, Italy
^{50c}INFN, I-10125, Turin, Italy
⁵¹Uppsala University, Box 516, SE-75120 Uppsala, Sweden
⁵²Wuhan University, Wuhan 430072, People's Republic of China

⁵³Zhejiang University, Hangzhou 310027, People's Republic of China
⁵⁴Zhengzhou University, Zhengzhou 450001, People's Republic of China
 (Received 21 February 2017; published 24 April 2017)

Using an electron-positron collision data sample of 2.93 fb^{-1} collected at a center-of-mass energy of $\sqrt{s} = 3.773 \text{ GeV}$ with the BESIII detector, we present the first search for the radiative leptonic decay $D^+ \rightarrow \gamma e^+ \nu_e$. The analysis is performed with a double-tag method. We do not observe a significant $D^+ \rightarrow \gamma e^+ \nu_e$ signal, and obtain an upper limit on the branching fraction of $D^+ \rightarrow \gamma e^+ \nu_e$ decay with the energy of radiative photon larger than 10 MeV of 3.0×10^{-5} at the 90% confidence level.

DOI: 10.1103/PhysRevD.95.071102

I. INTRODUCTION

In contrast to the purely leptonic decay, the radiative leptonic decay of the charged charmed meson, $D^+ \rightarrow \gamma e^+ \nu_e$, is not subject to the helicity suppression rule due to the presence of a radiative photon. With no final-state hadron, treatment of the nonperturbative strong interaction effects in theoretical calculations is relatively simple.

The radiative leptonic decays of heavy mesons have been studied with various models [1–4]. Within the perturbative quantum chromodynamics (pQCD) approach, the branching fraction of $D^+ \rightarrow \gamma e^+ \nu_e$ decay is predicted to be of order 10^{-4} [1]. Much smaller branching fractions, of order 10^{-6} , are obtained within the light front quark model [2] and the nonrelativistic constituent quark model [3]. In Ref. [4], the long-distance contribution is considered via the vector meson dominance model and it is found that the decay rate may be enhanced significantly. To deal with nonperturbative effects, it is important to separate the hard and soft physics, typically with an approach known as factorization. Many approaches to factorization of the radiative leptonic decays of heavy mesons have been proposed [5–11]. In recent papers [12,13], factorization is extended to consider the first-order corrections in the strong coupling constant α_s and the heavy quark mass; the branching fraction of $D^+ \rightarrow \gamma e^+ \nu_e$ decay is predicted to be of order 10^{-5} .

In this paper, we present the first search for the decay $D^+ \rightarrow \gamma e^+ \nu_e$, based on a data sample of 2.93 fb^{-1} [14,15]

collected with the BESIII detector at a center-of-mass energy $\sqrt{s} = 3.773 \text{ GeV}$. No obvious signal is observed, and an upper limit on the branching fraction of $D^+ \rightarrow \gamma e^+ \nu_e$ decay is set at the 90% confidence level (C.L.). In this paper, charge conjugate modes are always implied.

II. THE BESIII DETECTOR AND DATA SET

The BESIII detector is a general purpose spectrometer with a geometrical acceptance of 93% of 4π . It consists of a main drift chamber (MDC) for measuring the momentum and specific ionization of charged particles in a 1 T solenoidal magnetic field, a time of flight (TOF) system to perform particle identification, and a CsI(Tl) electromagnetic calorimeter (EMC) for measurement of deposited shower energies. These components are surrounded by a multilayer resistive plate counter system, which is designed to identify the muons. A detailed description of the BESIII detector can be found in Ref. [16].

High-statistics Monte Carlo (MC) simulated data samples are used to determine the detection efficiency and to estimate potential background contamination. A GEANT4-based [17] MC simulation program is used to simulate the interactions of particles in the spectrometer and the detector response. For the production of $\psi(3770)$, KKMC [18] is used; it includes the effects of beam energy spread and initial-state radiation (ISR). The known decay modes are generated using EVTGEN [19,20] according to branching fractions from the Particle Data Group [21], and the remaining unknown decay modes are simulated by LUNDCHARM [22]. Final-state radiation (FSR) of charged tracks is incorporated with PHOTOS [23]. In modeling the signal events, the approach of Ref. [12] is adopted, where first-order effects in the strong coupling constant α_s and the heavy quark mass are considered. The minimum energy of the radiative photon is set at 10 MeV to avoid the infrared divergence for soft photons. For $D^+ \rightarrow \pi^0 e^+ \nu_e$ decay, which is an important background, an exclusive MC sample is generated by adopting the associated form-factor model and parameters in Ref. [24].

III. $D^+ \rightarrow \gamma e^+ \nu_e$ DATA ANALYSIS

The analysis uses a double-tag (DT) technique [25] which exploits the exclusive $D\bar{D}$ final states produced near

*Also at Bogazici University, 34342 Istanbul, Turkey.
 †Also at Moscow Institute of Physics and Technology, Moscow 141700, Russia.
 ‡Also at Functional Electronics Laboratory, Tomsk State University, Tomsk, 634050, Russia.
 §Also at Novosibirsk State University, Novosibirsk 630090, Russia.
 ||Also at NRC “Kurchatov Institute,” PNPI, 188300 Gatchina, Russia.
 ¶Also at Istanbul Arel University, 34295 Istanbul, Turkey.
 **Also at Goethe University Frankfurt, 60323 Frankfurt am Main, Germany.
 ††Also at Key Laboratory for Particle Physics, Astrophysics and Cosmology, Ministry of Education; Shanghai Key Laboratory for Particle Physics and Cosmology; Institute of Nuclear and Particle Physics, Shanghai 200240, People's Republic of China.
 ‡‡Government College Women University, Sialkot 51310, Punjab, Pakistan.

threshold in e^+e^- experiments. This technique allows one to measure absolute decay branching fractions of D^+ mesons independent of any direct knowledge of the total number of D^+D^- events. In this analysis, the D^- candidates, so-called single-tag (ST) events, are reconstructed through six specific hadronic decay modes, $K^+\pi^-\pi^-$, $K^+\pi^-\pi^-\pi^0$, $K_S^0\pi^-$, $K_S^0\pi^-\pi^0$, $K_S^0\pi^+\pi^-\pi^-$ and $K^+K^-\pi^-$. The signal $D^+ \rightarrow \gamma e^+\nu_e$ is then searched for among the remaining tracks and showers recoiling against the ST D^- candidates; such signal candidate events are denoted as DT events. The absolute branching fraction, $\mathcal{B}(D^+ \rightarrow \gamma e^+\nu_e)$, can be obtained from the ratio of the DT yields and the ST yields,

$$\mathcal{B}(D^+ \rightarrow \gamma e^+\nu_e) = \frac{N_{\text{DT}}}{\sum_i N_{\text{ST}}^i \varepsilon_{\text{DT}}^i / \varepsilon_{\text{ST}}^i}, \quad (1)$$

where N_{DT} is the sum of signals yields for all tag modes and N_{ST}^i , $\varepsilon_{\text{DT}}^i$ and $\varepsilon_{\text{ST}}^i$ are the ST yields and the detection efficiencies of DT and ST for ST mode i , respectively. With this approach, the systematic uncertainties in the ST selection reconstruction are largely canceled in the branching fraction measurement.

A. Single-tag event selection and yields

For each charged track, we require the polar angle θ in the MDC to satisfy $|\cos\theta| < 0.93$ and the point of the closest approach to the interaction point (IP) of the e^+e^- beams to be within 1 cm in the plane perpendicular to the beam (V_r) and within ± 10 cm along the beam axis (V_z). Particle identification (PID) for charged tracks is accomplished by combining the information on the measured ionization energy loss (dE/dx) in the MDC and the flight time in the TOF into a PID likelihood, $\mathcal{L}(h)$, for each hadron hypothesis $h = K$ or $h = \pi$. The π (K) candidates are required to satisfy $\mathcal{L}(\pi) > \mathcal{L}(K)$ [$\mathcal{L}(K) > \mathcal{L}(\pi)$].

The K_S^0 candidates are reconstructed from combinations of two tracks with opposite charge which satisfy $|\cos\theta| < 0.93$ and $|V_z| < 20$ cm, but with no V_r and no PID requirements. The K_S^0 candidates must have an invariant mass in the range $0.487 < M_{\pi^+\pi^-} < 0.511$ GeV/ c^2 , corresponding to three times our mass resolution. To reject combinatorial background, we further require the decay length of K_S^0 candidates, the distance between the IP and the reconstructed secondary decay vertex provided by a vertex fit algorithm, to be larger than 2 standard deviations. The momenta of $\pi^+\pi^-$ pairs after the vertex fit are used in subsequent analysis.

Those showers deposited in the EMC not associated with charged tracks are identified as photon candidates. The energy deposited in the nearby TOF counters is included to improve energy resolution and detection efficiency. The minimum deposited energy is required to be greater than 25 MeV in the barrel region ($|\cos\theta| < 0.80$), or 50 MeV in the end cap regions ($0.84 < |\cos\theta| < 0.92$). The shower time is required to be within 700 ns after the event start

TABLE I. Summary of the ΔE requirements, ST yields N_{ST}^i in data and detection efficiencies $\varepsilon_{\text{ST}}^i$. The efficiencies do not include the branching fractions of $K_S^0 \rightarrow \pi^+\pi^-$ and $\pi^0 \rightarrow \gamma\gamma$. All uncertainties are statistical only.

Tag mode	ΔE (MeV)	N_{ST}^i	$\varepsilon_{\text{ST}}^i$ (%)
$K^+\pi^-\pi^-$	[-27, 25]	801498 ± 940	51.57 ± 0.02
$K^+\pi^-\pi^-\pi^0$	[-62, 34]	242092 ± 699	24.37 ± 0.02
$K_S^0\pi^-$	[-25, 25]	98132 ± 328	54.03 ± 0.06
$K_S^0\pi^-\pi^0$	[-73, 41]	213976 ± 641	26.17 ± 0.02
$K_S^0\pi^+\pi^-\pi^-$	[-33, 30]	127463 ± 415	32.46 ± 0.04
$K^+K^-\pi^-$	[-23, 20]	70701 ± 343	41.83 ± 0.06

time to suppress electronic noise and showers unrelated to the collision event. The π^0 candidates are reconstructed from pairs of photons with invariant mass satisfying $0.115 < M_{\gamma\gamma} < 0.150$ GeV/ c^2 ; those with both photons in the EMC end caps are rejected because of poorer resolution. The photon pairs of π^0 candidates are subject to a one-constraint (1C) kinematic fit which constrains their mass to the nominal π^0 mass [21]; the updated momenta are used in subsequent analysis.

The ST D^- signals are discriminated from backgrounds based on two kinematic variables, the energy difference, ΔE , and the beam-constrained mass, M_{BC} (encompassing energy and momentum conservation), which are defined as

$$\Delta E \equiv E_{\text{ST}} - E_{\text{beam}}, \quad (2)$$

$$M_{\text{BC}} \equiv \sqrt{E_{\text{beam}}^2/c^4 - |\vec{p}_{\text{ST}}|^2/c^2}, \quad (3)$$

where \vec{p}_{ST} and E_{ST} are the total momentum and energy of the ST D^- candidate in the rest frame of the e^+e^- system, respectively, and E_{beam} is the beam energy. The ST signals peak around zero in the ΔE distribution and around the nominal D^- mass [21] in the M_{BC} distribution.

For each ST mode, the D^- candidates are reconstructed from all possible combinations of final-state particles, and are required to have ΔE within the regions listed in Table I; these are final-state dependent and determined from data. If multiple candidates are found, only the one with the smallest $|\Delta E|$ is selected. To extract the ST signal yields, we perform extended unbinned maximum likelihood fits to the M_{BC} distributions, as shown in Fig. 1. In the fits, signal shapes derived from the signal MC events are convoluted with a Gaussian function; the free mean and width of this Gaussian compensate for imperfections in the beam energy calibration and differences in the detector resolution between data and MC simulation, respectively. The combinatorial background is modeled by a smooth ARGUS function [26]. The signal yields and the corresponding detection efficiencies in the region $1.8628 < M_{\text{BC}} < 1.8788$ GeV/ c^2 are summarized in Table I. A study of

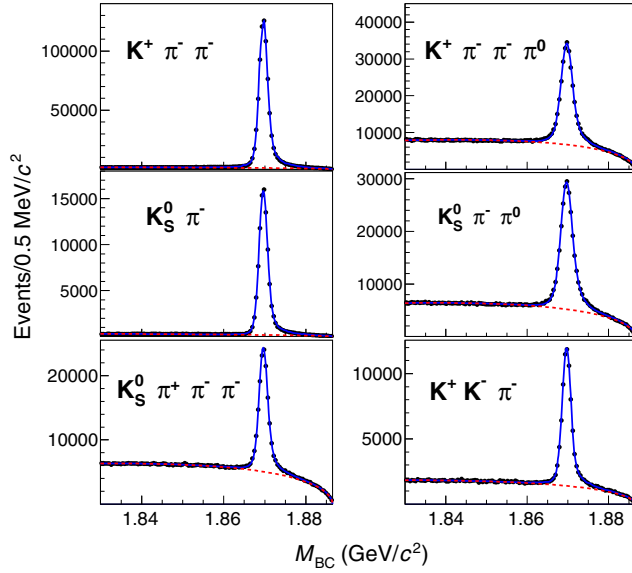


FIG. 1. The M_{BC} distributions for the six tag modes. Dots with error bars are data. The blue solid lines show the overall fit curves and the red dashed lines are for the background contributions.

the inclusive $D\bar{D}$ MC samples, in which both D mesons decay inclusively, indicates that there are no significant backgrounds which peak in M_{BC} .

B. Double-tag event selection and yields

We search for the signal $D^+ \rightarrow \gamma e^+ \nu_e$ in the remaining charged tracks and showers recoiling against the ST D^- candidates. Exactly one good remaining charged track is required, with charge opposite to that of the ST D^- . The track must be identified as an electron by combining the information from dE/dx , TOF and the EMC. The PID \mathcal{L} is required to satisfy $\mathcal{L}(e) > 0$ and $\mathcal{L}(e)/(\mathcal{L}(e) + \mathcal{L}(\pi) + \mathcal{L}(K)) > 0.8$. There must be at least one remaining photon to be selected as the candidate radiative photon. The selection criteria of good photons are the same with those for the ST side; in the case of multiple candidates, the highest energy photon is used. However, we reject events in which any pair of photons satisfies $\chi^2 < 20$ in the π^0 1C kinematic fit. To improve the degraded momentum resolution of the electron due to FSR and bremsstrahlung, the energy of neighboring photons, presumably due to FSR, is added back to electron candidates. Specifically, photons with energy greater than 50 MeV and within a cone of 5° around the electron direction (but excluding the radiative one) are included. To suppress the background $D^+ \rightarrow K_L^0 e^+ \nu_e$, the radiative photon is further required to have a lateral moment [27] within the range (0.0, 0.3). This lateral moment, which describes the shape of electromagnetic showers, is found in MC event studies to peak around 0.15 for photons but to vary broadly from 0 to 0.85 for K_L^0 candidates.

In the selection of DT events, the undetected neutrino is inferred by studying the missing energy, E_{miss} , and missing momentum, \vec{p}_{miss} , which are defined as

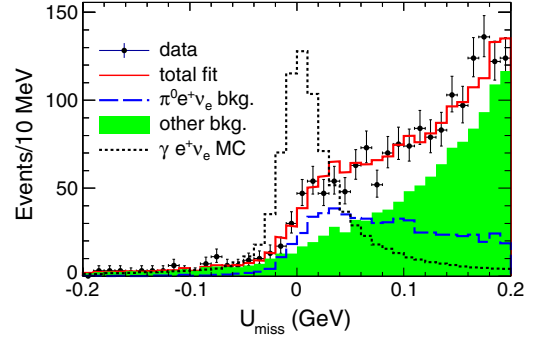


FIG. 2. The U_{miss} distribution. Dots with error bars are data, the red solid-line histogram shows the overall fit curve, the blue dashed-line histogram shows the background $D^+ \rightarrow \pi^0 e^+ \nu_e$, and the green shaded histogram includes all other background. The black dotted line shows the signal MC simulation normalized to the branching fraction $\mathcal{B}(D^+ \rightarrow \gamma e^+ \nu_e) = 100 \times 10^{-5}$.

$$E_{\text{miss}} \equiv E_{\text{beam}} - E_\gamma - E_e, \quad (4)$$

and

$$\vec{p}_{\text{miss}} \equiv -\left[\vec{p}_\gamma + \vec{p}_e + \hat{p}_{\text{ST}} \sqrt{E_{\text{beam}}^2/c^2 - m_{D^-}^2 c^2}\right], \quad (5)$$

in the rest frame of e^+e^- system. Here, E_γ (E_e) and \vec{p}_γ (\vec{p}_e) are the energy and momentum of the radiative photon (electron), respectively, and m_{D^-} is the nominal mass of the D^- meson [21]. In calculating \vec{p}_{miss} , only the direction vector of the ST D^- candidate, \hat{p}_{ST} , is used; the corresponding magnitude of momentum is fixed. The variable U_{miss} is then defined as

$$U_{\text{miss}} \equiv E_{\text{miss}} - |\vec{p}_{\text{miss}}|c. \quad (6)$$

The distribution of U_{miss} for the surviving DT candidates is illustrated in Fig. 2; the $D^+ \rightarrow \gamma e^+ \nu_e$ signals should peak around zero, as shown with the dotted curve.

By studying the MC simulation samples, the background from the semileptonic decay $D^+ \rightarrow \pi^0 e^+ \nu_e$ is found to have a nontrivial shape in U_{miss} . Therefore, we study the $D^+ \rightarrow \pi^0 e^+ \nu_e$ backgrounds exclusively by selecting a control sample in data with exactly the same selection criteria for the ST events and electron candidates used in the selection of signal events. The π^0 candidates are reconstructed from two photons with a 1C kinematic fit constraining their mass to the π^0 nominal value and having a fit $\chi^2 < 20$. We extract the yield of the control sample $D^+ \rightarrow \pi^0 e^+ \nu_e$, $N_{\text{DT}}^{\pi^0}$, by fitting the corresponding U_{miss} distribution. The expected number of background $D^+ \rightarrow \pi^0 e^+ \nu_e$ in the selection of signal $D^+ \rightarrow \gamma e^+ \nu_e$, $N_{\pi^0}^{\text{exp}}$, is calculated with

$$N_{\pi^0}^{\text{exp}} = \frac{N_{\text{DT}}^{\pi^0}}{\sum_i \frac{N_{\text{ST}}^i}{\epsilon_{\text{ST}}^i} \epsilon_{\text{DT},\pi^0}^i} \sum_i \frac{N_{\text{ST}}^i}{\epsilon_{\text{ST}}^i} \epsilon_{\text{DT},\pi^0}^i, \quad (7)$$

TABLE II. Summaries of the DT efficiencies of $D^+ \rightarrow \gamma e^+ \nu_e$ (ϵ_{DT}^i) and $D^+ \rightarrow \pi^0 e^+ \nu_e$ ($\epsilon_{\text{DT},\pi^0}^i$), and the rates of misidentifying $D^+ \rightarrow \pi^0 e^+ \nu_e$ as $D^+ \rightarrow \gamma e^+ \nu_e$ ($\epsilon_{\text{DT},\pi^0}^{i,\gamma}$), where the branching fraction of $K_S^0 \rightarrow \pi^+ \pi^-$ and $\pi^0 \rightarrow \gamma\gamma$ are not included. The uncertainties are MC statistical only.

Tag mode	ϵ_{DT}^i (%)	$\epsilon_{\text{DT},\pi^0}^i$ (%)	$\epsilon_{\text{DT},\pi^0}^{i,\gamma}$ (%)
$K^+ \pi^- \pi^-$	27.09 ± 0.11	27.93 ± 0.14	5.32 ± 0.07
$K^+ \pi^- \pi^- \pi^0$	14.28 ± 0.08	13.79 ± 0.11	3.05 ± 0.05
$K_S^0 \pi^-$	28.97 ± 0.10	30.23 ± 0.14	5.87 ± 0.07
$K_S^0 \pi^- \pi^0$	15.62 ± 0.08	15.17 ± 0.11	3.29 ± 0.06
$K_S^0 \pi^+ \pi^- \pi^-$	17.86 ± 0.09	17.55 ± 0.12	3.72 ± 0.06
$K^+ K^- \pi^-$	21.12 ± 0.10	22.28 ± 0.13	4.19 ± 0.06

where $\epsilon_{\text{DT},\pi^0}^i$ is the DT efficiency of $D^+ \rightarrow \pi^0 e^+ \nu_e$, $\epsilon_{\text{DT},\pi^0}^{i,\gamma}$ is the rate of misidentifying $D^+ \rightarrow \pi^0 e^+ \nu_e$ as $D^+ \rightarrow \gamma e^+ \nu_e$ for the tag mode i , individually. The values of the corresponding efficiencies are summarized in Table II. We find $N_{\text{DT}}^{\pi^0} = 3016 \pm 68$ and $N_{\pi^0}^{\text{exp}} = 612 \pm 14$, respectively, where the errors are statistical only.

An extended unbinned maximum likelihood fit is performed on the final U_{miss} distribution as shown in Fig. 2. The signal shape is derived from the simulated $D^+ \rightarrow \gamma e^+ \nu_e$ events convoluted with a Gaussian function to compensate for resolution differences between data and MC simulation. The parameters of this Gaussian smearing function are extracted according to the discrepancy in resolution between data and MC simulation in the control sample $D^+ \rightarrow \pi^0 e^+ \nu_e$, and are fixed in the fit. The shape of the background $D^+ \rightarrow \pi^0 e^+ \nu_e$ is extracted from the simulated $D^+ \rightarrow \pi^0 e^+ \nu_e$ sample, and is normalized to $N_{\pi^0}^{\text{exp}}$. For the other background components, the shape from the inclusive MC sample (excluding the contribution from $D^+ \rightarrow \pi^0 e^+ \nu_e$) is adopted and the yield is determined in the fit. We obtain a signal yield of $N_{\text{DT}} = -21 \pm 23$, and the resulting branching fraction is $\mathcal{B}(D^+ \rightarrow \gamma e^+ \nu_e) = (-2.5 \pm 2.7) \times 10^{-5}$, where the uncertainties are statistical only. Since no obvious signal is observed, an upper limit at the 90% C.L. on the branching fraction of $D^+ \rightarrow \gamma e^+ \nu_e$ will be set below after taking into account the effects of statistical and systematic uncertainties.

IV. SYSTEMATIC UNCERTAINTIES

The systematic uncertainties in the selection of the ST candidates are assumed to largely cancel, with any residual effects being negligible. Other systematic uncertainties, related to the detection efficiencies, are summarized in Table III. To evaluate the systematic uncertainty related to the model of the decay dynamics, an alternative signal MC sample based on the single-pole model [1,12] is produced, and the resultant difference in the detection efficiency with respect to the nominal value, 3.5%, is assigned as the

TABLE III. Systematic uncertainties related to detection efficiencies in the branching fraction measurement.

Source	Relative uncertainty (%)
Signal MC model	3.5
e^+ tracking	0.5
e^+ PID	0.5
γ reconstruction	1.0
Lateral moment	4.4
$\pi^0 e^+ \nu_e$ backgrounds	2.7 ^a

^aNote that this value is a fractional change in the $\pi^0 e^+ \nu_e$ rate, not in the branching fraction of $D^+ \rightarrow \gamma e^+ \nu_e$.

systematic uncertainty. The uncertainties of electron tracking and PID are estimated to be 0.5% and 0.5%, respectively, by studying a control sample of radiative Bhabha scattering events. The uncertainty in photon reconstruction is assigned as 1.0%, based on a study of double-tagged $D^0 \rightarrow K_S \pi^0$ events [28]. The uncertainty related with the lateral moment requirement for the photon is estimated to be 4.4% by studying a photon control sample from radiative Bhabha scattering events. The quadratic sum of the above systematic uncertainties, related to detection efficiency, is 5.8%.

The systematic uncertainty associated with the estimated number of background $D^+ \rightarrow \pi^0 e^+ \nu_e$ events includes a statistical uncertainty on the size of the DT control sample ($D^+ \rightarrow \pi^0 e^+ \nu_e$) of 2.3%, and relative uncertainties on the detection efficiency relative to signal of 1.0% for the π^0 1C kinematic fit and 1.0% for the extra photon with respect to the signal. Adding in quadrature, the total uncertainty of the background $D^+ \rightarrow \pi^0 e^+ \nu_e$ rate is 2.7%. Note this value is not the direct fractional change in the branching fraction of $D^+ \rightarrow \gamma e^+ \nu_e$; it is the fluctuation of background $D^+ \rightarrow \pi^0 e^+ \nu_e$ and will be considered along with other effects from the fit procedure.

Various sources of systematic uncertainties in the fit procedure are considered: (a) fits are redone with the fitting range being as $(-0.15, 0.25)$ GeV or $(-0.20, 0.25)$ GeV, (b) the mean and width of the smearing Gaussian function for the signal shape are varied according to the corresponding uncertainties obtained from the control sample $D^+ \rightarrow \pi^0 e^+ \nu_e$, (c) the number of the background $D^+ \rightarrow \pi^0 e^+ \nu_e$ is varied according its uncertainty (2.7%), and (d) the shape derived from the inclusive MC sample is replaced by a second-order polynomial function to describe the other backgrounds excluding $D^+ \rightarrow \pi^0 e^+ \nu_e$. All of these fitting procedure effects are accounted for within the upper limit evaluation described next.

V. THE UPPER LIMIT ON THE BRANCHING FRACTION

To set the upper limit on the decay branching fraction $\mathcal{B}(D^+ \rightarrow \gamma e^+ \nu_e)$, we follow the method in Refs. [28,29]

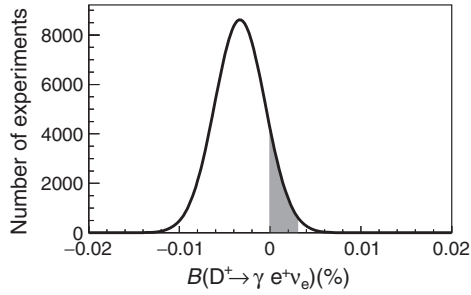


FIG. 3. Distribution of the accumulated branching fraction based on toy MC samples generated according to the data. The shaded region represents 90% of the physical region.

which takes into account the effects of both systematic and statistical uncertainties. We obtain a smooth probability density function (PDF) from the data sample using the kernel estimation method [30]. A large number of toy MC samples are generated according to the smooth PDF, while the number of events in each MC sample is allowed to fluctuate with a Poisson distribution according to the yield found in the fit to the data sample. The same fit procedure used for data is applied to each toy MC sample, while randomly making systematic variations in the fit procedure, as described in the previous section. In the calculation of the branching fraction $\mathcal{B}(D^+ \rightarrow \gamma e^+ \nu_e)$ for the toy MC sample, the DT efficiencies are varied randomly according to the detection efficiency uncertainties (5.8%), and the ST yields and the corresponding efficiencies are varied randomly according to the statistical uncertainty due to the size of data and MC samples. The resultant distribution of $\mathcal{B}(D^+ \rightarrow \gamma e^+ \nu_e)$ for all toy MC samples is shown in Fig. 3. By integrating up to 90% of the area in the physical region $\mathcal{B}(D^+ \rightarrow \gamma e^+ \nu_e) \geq 0$, we obtain an upper limit at the 90% C.L. for the branching fraction as $\mathcal{B}(D^+ \rightarrow \gamma e^+ \nu_e) < 3.0 \times 10^{-5}$.

VI. SUMMARY

In summary, we present the first search for the radiative leptonic decay $D^+ \rightarrow \gamma e^+ \nu_e$ in the charm sector based on a DT method using a data sample of 2.93 fb^{-1} collected with the BESIII detector at a center-of-mass energy $\sqrt{s} = 3.773 \text{ GeV}$. No significant $D^+ \rightarrow \gamma e^+ \nu_e$ signal is

observed. With a 10 MeV cutoff on the radiative photon energy, the upper limit of the decay branching fraction for $D^+ \rightarrow \gamma e^+ \nu_e$ is $\mathcal{B}(D^+ \rightarrow \gamma e^+ \nu_e) < 3.0 \times 10^{-5}$ at the 90% C.L. The result approaches the theoretical predictions in Refs. [12,13]; more data may help to discriminate among the full suite of theoretical models.

ACKNOWLEDGMENTS

The BESIII collaboration thanks the staff of BEPCII and the IHEP computing center for their strong support. This work is supported in part by National Key Basic Research Program of China under Contract No. 2015CB856700; National Natural Science Foundation of China (NSFC) under Contracts No. 11125525, No. 11235011, No. 11275266, No. 11322544, No. 11335008, No. 11425524, and No. 11635010; the Chinese Academy of Sciences (CAS) Large-Scale Scientific Facility Program; the CAS Center for Excellence in Particle Physics (CCEPP); the Collaborative Innovation Center for Particles and Interactions (CICPI); Joint Large-Scale Scientific Facility Funds of the NSFC and CAS under Contracts No. U1232201, No. U1332201, No. U1532257, and No. U1532258; CAS under Contracts No. KJCX2-YW-N29, No. KJCX2-YW-N45, and No. QYZDJ-SSW-SLH003; 100 Talents Program of CAS; National 1000 Talents Program of China; INPAC and Shanghai Key Laboratory for Particle Physics and Cosmology; German Research Foundation DFG under Contracts No. Collaborative Research Center CRC 1044 and No. FOR 2359; Istituto Nazionale di Fisica Nucleare, Italy; Koninklijke Nederlandse Akademie van Wetenschappen (KNAW) under Contract No. 530-4CDP03; Ministry of Development of Turkey under Contract No. DPT2006K-120470; the Swedish Research Council; U.S. Department of Energy under Contracts No. DE-FG02-05ER41374, No. DE-SC-0010504, No. DE-SC-0010118, and No. DE-SC-0012069; U.S. National Science Foundation; University of Groningen (RuG) and the Helmholtzzentrum fuer Schwerionenforschung GmbH (GSI), Darmstadt; WCU Program of National Research Foundation of Korea under Contract No. R32-2008-000-10155-0.

-
- [1] G. Burdman, T. Goldman, and D. Wyler, *Phys. Rev. D* **51**, 111 (1995).
 [2] C. Q. Geng, C. C. Lih, and W.-M. Zhang, *Mod. Phys. Lett. A* **15**, 2087 (2000).
 [3] C.-D. Lü and G.-L. Song, *Phys. Lett. B* **562**, 75 (2003).

- [4] J.-C. Yang and M.-Z. Yang, *Mod. Phys. Lett. A* **27**, 1250120 (2012).
 [5] G. P. Korchemsky, D. Pirjol, and T.-M. Yan, *Phys. Rev. D* **61**, 114510 (2000).
 [6] S. Descotes-Genon and C. T. Sachrajda, *Nucl. Phys.* **B650**, 356 (2003).

M. ABLIKIM *et al.*

PHYSICAL REVIEW D **95**, 071102(R) (2017)

- [7] S. W. Bosch, R. J. Hill, B. O. Lange, and M. Neubert, *Phys. Rev. D* **67**, 094014 (2003).
- [8] R. J. Hill and M. Neubert, *Nucl. Phys.* **B657**, 229 (2003).
- [9] E. Lunghi, D. Pirjol, and D. Wyler, *Nucl. Phys.* **B649**, 349 (2003).
- [10] J. Ma and Q. Wang, *J. High Energy Phys.* 01 (2006) 067.
- [11] Y.-M. Wang, *J. High Energy Phys.* 09 (2016) 159.
- [12] J.-C. Yang and M.-Z. Yang, *Nucl. Phys.* **B889**, 778 (2014).
- [13] J.-C. Yang and M.-Z. Yang, *Nucl. Phys.* **B914**, 301 (2017).
- [14] M. Ablikim *et al.* (BESIII Collaboration), *Chin. Phys. C* **37**, 123001 (2013).
- [15] M. Ablikim *et al.* (BESIII Collaboration), *Phys. Lett. B* **753**, 629 (2016).
- [16] M. Ablikim *et al.* (BESIII Collaboration), *Nucl. Instrum. Methods Phys. Res., Sect. A* **614**, 345 (2010).
- [17] S. Agostinelli *et al.* (GEANT4 Collaboration), *Nucl. Instrum. Methods Phys. Res., Sect. A* **506**, 250 (2003).
- [18] S. Jadach, B. F. L. Ward, and Z. Was, *Phys. Rev. D* **63**, 113009 (2001).
- [19] P. Rong-Gang, *Chin. Phys. C* **32**, 599 (2008).
- [20] D. J. Lange, *Nucl. Instrum. Methods Phys. Res., Sect. A* **462**, 152 (2001).
- [21] J. Beringer *et al.* (Particle Data Group Collaboration), *Phys. Rev. D* **86**, 010001 (2012).
- [22] J. C. Chen, G. S. Huang, X. R. Qi, D. H. Zhang, and Y. S. Zhu, *Phys. Rev. D* **62**, 034003 (2000).
- [23] E. Richter-Was, *Phys. Lett. B* **303**, 163 (1993).
- [24] D. Besson *et al.* (CLEO Collaboration), *Phys. Rev. D* **80**, 032005 (2009).
- [25] R. M. Baltrusaitis *et al.* (MARK-III Collaboration), *Phys. Rev. Lett.* **56**, 2140 (1986).
- [26] H. Albrecht *et al.* (ARGUS Collaboration), *Phys. Lett. B* **241**, 278 (1990).
- [27] A. Drescher, B. Gräwe, B. Hahn, B. Ingelbach, U. Matthiesen, H. Scheck, J. Spengler, and D. Wegener, *Nucl. Instrum. Methods Phys. Res., Sect. A* **237**, 464 (1985).
- [28] M. Ablikim *et al.* (BESIII Collaboration), *Phys. Rev. D* **91**, 112015 (2015).
- [29] J. P. Lees *et al.* (BABAR Collaboration), *Phys. Rev. D* **85**, 091107 (2012).
- [30] K. S. Cranmer, *Comput. Phys. Commun.* **136**, 198 (2001).